Lab on a Chip

Devices and applications at the micro- and nanoscale

rsc.li/loc

ROYAL SOCIETY
OF **CHEMISTRY**
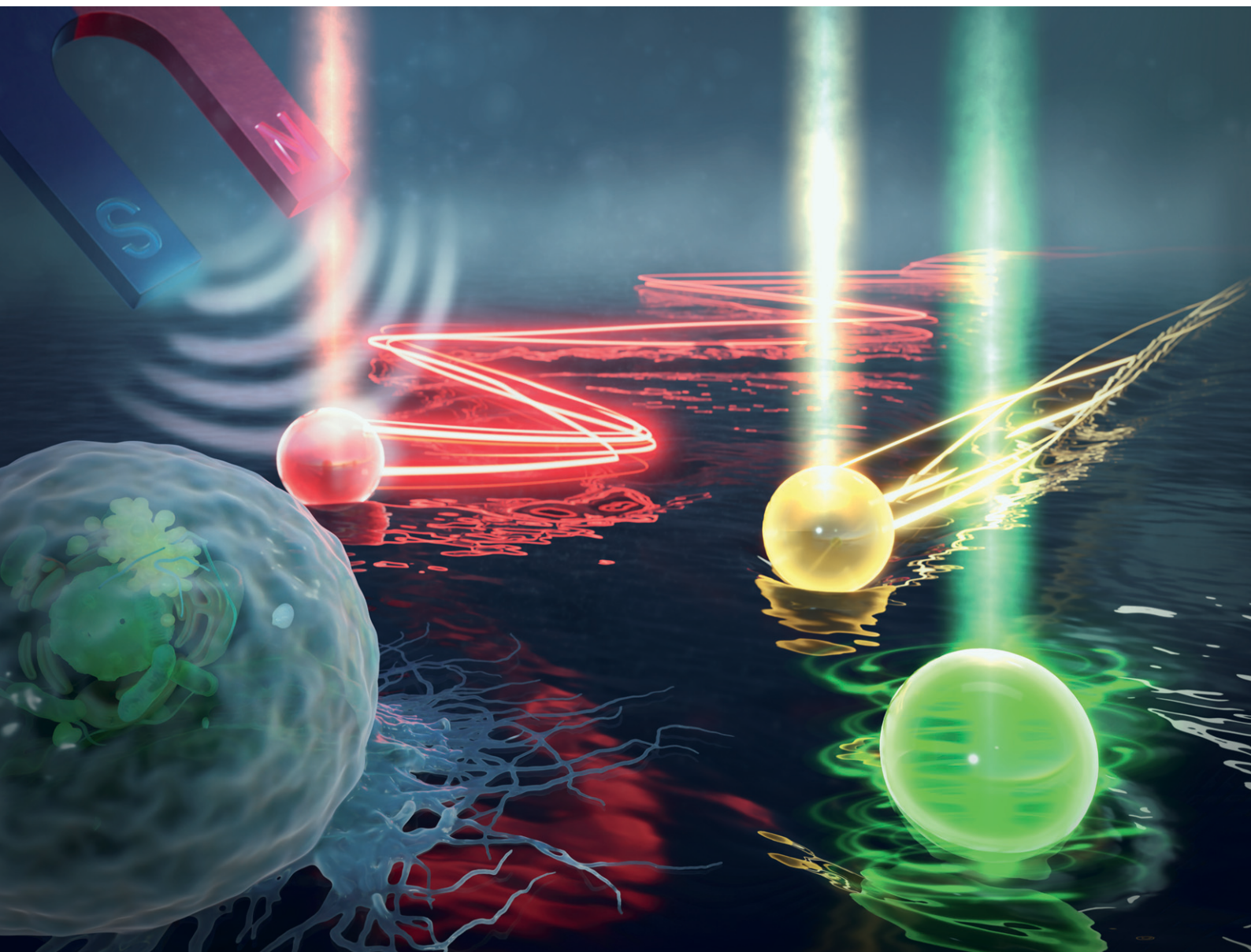
PAPER
Shilun Feng, Yu-Cheng Chen *et al.*
Motor-like microlasers functioning in biological fluids

Motor-like microlasers functioning in biological fluids†

Ziyihui Wang, [iD] [ab] Linwei Shang, [b] Zehang Gao, [iD] [cd] Kok Ken Chan, [b] Chaoyang Gong, [b] Chenlu Wang, [b] Tianhua Xu, [iD] [ae] Tiegen Liu, [a] Shilun Feng*[c] and Yu-Cheng Chen [iD] *[b]

Microlasers integrated with biological systems have received tremendous attention for their intense light intensity and narrow linewidth recently, serving as a powerful tool for studying complex dynamics and interactions in scattered biological micro-environments. However, manipulation of microlasers with controllable motions and versatile functions remains elusive. Herein, we introduce the concept of motor-like microlasers formed by magnetic-doped liquid crystal droplets, in which the direction and velocity could be controlled by altering internal magnetic nanoparticles or external magnetic fields. Both translational and rotatory motions of the lasing resonator could be continually changed in real-time. Lasing-encoded motors carrying different functions and lasing wavelengths were also achieved. Finally, we demonstrate the potential of motor-like microlasers by functioning as a localized stimulation emission light source to stimulate or illuminate living cells, providing a novel approach for switching on/off light emissions and subcellular imaging. Laser emitting micromotors offer a facile system for precise manipulation of microlasers in biological fluids, providing new insight into the development of programmable on-chip laser devices and laser-emitting intelligent systems.

Introduction

With the recent emergence of robotics, robots and motors have been widely developed in various manners, particularly in industrial, medical, and environmental applications.[1,2] The

[a] *School of Precision Instrument and Opto-Electronics Engineering, Tianjin University, Tianjin 300072, China*

[b] *School of Electrical and Electronics Engineering, Nanyang Technological University, 50 Nanyang Ave., Singapore 639798, Singapore. E-mail: yucchen@ntu.edu.sg*

[c] *State Key Laboratory of Transducer Technology, Shanghai Institute of Microsystem and Information Technology, Chinese Academy of Science, Shanghai, 200050, China. E-mail: shilun.feng@mail.sim.ac.cn*

[d] *Department of Clinical Laboratory, Third Affiliated Hospital of Guangzhou Medical University, Guangdong 510150, China*

[e] *School of Engineering, University of Warwick, Coventry, CV4 7AL, UK*

† Electronic supplementary information (ESI) available: Movement performance of the lasing micromotor after 90 days of storage; photoluminescence spectra and lasing emission behavior of the micromotor; magneto-switchable behaviors of the lasing micromotor; absorption and emission spectra of the dyes doped in the micromotor; image processing of the lasing micromotor captured with a galvo-scanner (PDF). Performance of the lasing after 90 days of storage (MP4). Self-rotation of the lasing micromotor (MP4). Propelled motion of the lasing micromotor under the guidance of various magnetic fields (MP4). Micromotor with different magnetic nanoparticle loading percentages (MP4). Magneto-switchable behaviors (MP4). Letters "N", "T", and "U" written by the multiple lasing micromotor (MP4). Recording of the multicolored micromotor exhibited different velocities (MP4). See DOI: https://doi.org/10.1039/d2lc00513a

scale of motors has also shrunk down to the microscale in the last decade, where micromotors can be manipulated by optical tweezers, magnetic forces, acoustic waves, and even chemical reactions.[3–12] Direct visualization and tracking of these mobile systems are crucial for studying complex dynamics and interactions. An emerging approach is the design of dynamic devices that couple mechanical motion and light emission;[13,14] for instance, many photoluminescent motors have been developed through the incorporation of dyes or photoluminescent materials.[15,16] However, these motors generally have a broad spectrum and relatively low intensity. To date, light-emitting motors have been mostly employed as a passive light source, where the photoluminescence serves as an indicator for tracking or visualization in a liquid environment.

Compared to conventional light sources, laser emission (stimulated emission) generated through the optical feedback provided by the resonator exhibits a strong light intensity, narrow linewidth, and high signal-to-noise ratio.[17,18] Microlasers integrated with biological systems have thus received tremendous attention for their potential in biological applications, serving as a powerful tool for studying complex dynamics in scattered biological micro-environments.[19–25] Recent studies have also incorporated microlasers with cells or tissues, aiming to reveal biological behaviours at the cellular level.[26–30] In spite of the progress

that has been developed,[31–34] manipulation of microlasers under large dimensions with controllable and versatile functions remains a key challenge. Exploring a versatile way for driving and controlling coherent light sources in a liquid environment holds great potential in photostimulation and photoactivable reactions.

In this study, we introduce the concept of a motor-like microlaser (or lasing micromotor), in which the direction, velocity, and spatial motions of a microlaser resonator could be fully controlled and programmed. As illustrated in Fig. 1a, microlasers supported by whispering gallery modes (WGM) are formed by cholesteric liquid crystal (CLC) droplets encapsulated with magnetic nanoparticles (MNPs). For the first attempt, the motion of the lasing micromotor could be manipulated in biological fluids in two dimensions (X-axis and Y-axis) under the efficient guidance of a magnetic field. Besides linear motion, spinning and rotatory motions were achieved. Here we demonstrate that the velocity of the lasing micromotor could be regulated by either loading different concentrations of MNPs in droplets or by changing the strength of external magnetic fields. The ability to manipulate microlasers in biological fluids thus opens new possibilities in biophotonic applications. As a proof-of-concept, herein, we showcase the potential functions of the lasing micromotor by utilizing it as a localized stimulated emission source for on-chip laser writing as well as for switching on/off adjacent emissive particles. Finally, the lasing micromotor was employed as a localized laser probe to excite fluorescently labeled living cells, offering a facile strategy for localized single-cell modulation and imaging on-chip.

Results and discussion

To obtain monodisperse and uniform-sized particles (~30 μm), laser emitting CLC droplets were prepared using a homemade microfluidic chip. As illustrated in (Fig. 1b), magnetic particles were premixed in dye-doped CLC, serving as the oil phase, while poly(vinyl alcohol) (PVA) solution served as the water phase to form lasing microdroplets. The unique helical arrangement of chiral molecules in CLC provided a stable environment for encapsulating MNPs in lasing droplets, maintaining their performance even after 90 days (Fig. S2 and corresponding Video S1†). The lasing wavelength could be manipulated by changing the organic dyes (laser gain) in CLC droplets. For instance, blue, green, yellow, and red emission could be achieved at desired lasing wavelength according to the embedded dyes. The concentration of the embedded fluorescent dyes directly affects the lasing thresholds, and hence can also serve as a switch to control different lasing motors. Another method to adjust the lasing wavelength is to change the chiral dopant concentration in liquid crystal droplets. The unique properties of chiral molecules promote alignment variation of dye molecules which result in changes of optical absorption. A previous study has reported that WGM lasing
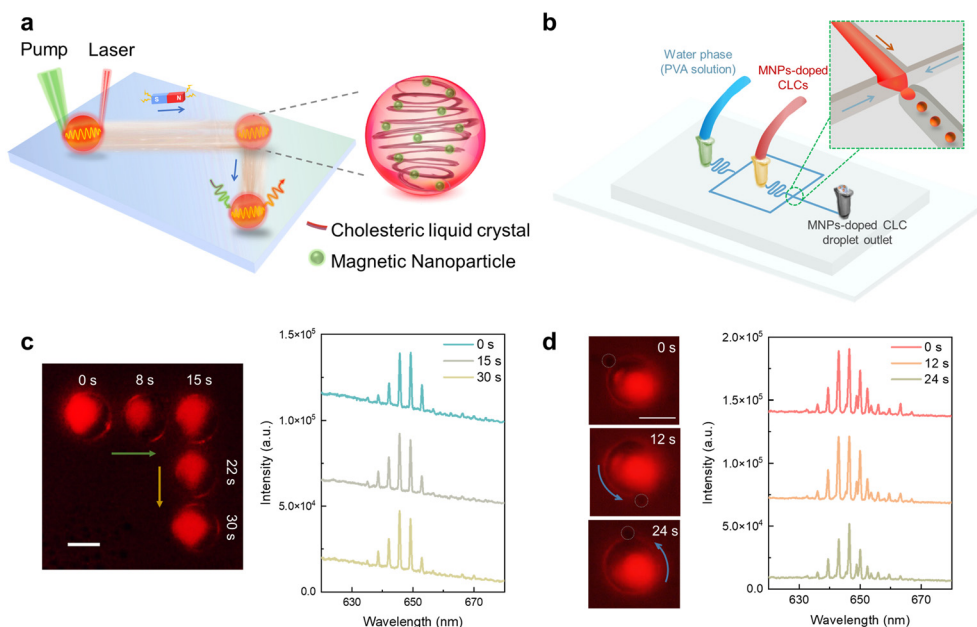
Fig. 1 (a) Schematic diagram of the lasing micromotor formed by cholesteric liquid crystal (CLC) droplets encapsulated with MNPs. The motion of the lasing micromotor can be precisely controlled through magnetic fields. (b) Illustration of lasing micromotor formation. (c) Left: Real-time positions of the Nile Red (NR)-doped lasing micromotor guided by the magnetic field (integrated through the same field of view alignment). Within 0–15 s, the direction of the magnetic field was along the green line; within 16–30 s, the direction of the magnetic field followed the yellow line. The motion of the lasing micromotor was always in accordance with the magnetic field. Right: WGM lasing spectrum recorded from the microlaser at different times. (d) Left: Self-rotation of the NR-doped lasing micromotor by employing the rotating magnetic field. The gray circle shows the position of the comparable reference attached to the lasing micromotor (refer to Fig. S1† for better observation of the reference position). Right panel: WGM lasing spectrum. Scale bar: 20 μm.

will shift toward long wavelengths (red shift) as the chiral dopant concentration increases.[35]

To verify the lasing action, we measured the output lasing intensities and linewidths of a microlaser droplet by increasing the pump energy densities in Fig. S3† (Nile Red (NR)-doped CLC droplet with MNPs). Spectrally integrated output intensity and linewidths were subsequently measured based on the spectra in Fig. S3a,† where the linewidth of the peak is defined by its full width at half maximum. As shown in Fig. S3b,† a clear threshold was observed for both the output intensities and linewidths. Linewidth narrowing was obtained when the pump energy density reaches above the lasing threshold. A bright ring shape pattern indicated the WGM photoemission guided by the total internal reflection along the edge of the

particle. Additionally, we compared the lasing thresholds and Q-factors for the lasing droplet with and without MNPs in Fig. S3.† A slightly higher lasing threshold and lower Q-factor were obtained due to scattering loss from magnetic nanoparticles throughout the WGM resonator.

With the guidance of magnetic fields, the direction and motion of lasing micromotors could be manipulated remotely. For instance, in Fig. 1c, the trajectory demonstrates the ability to control in *X* and *Y* directions, where the direction could be continually changed by adjusting the orientation of the magnet in real-time. The position of the lasing micromotor, as well as its lasing spectrum, was recorded at respective seconds, as shown in Fig. 1c. During continuous movement, the resonator remained spherical,
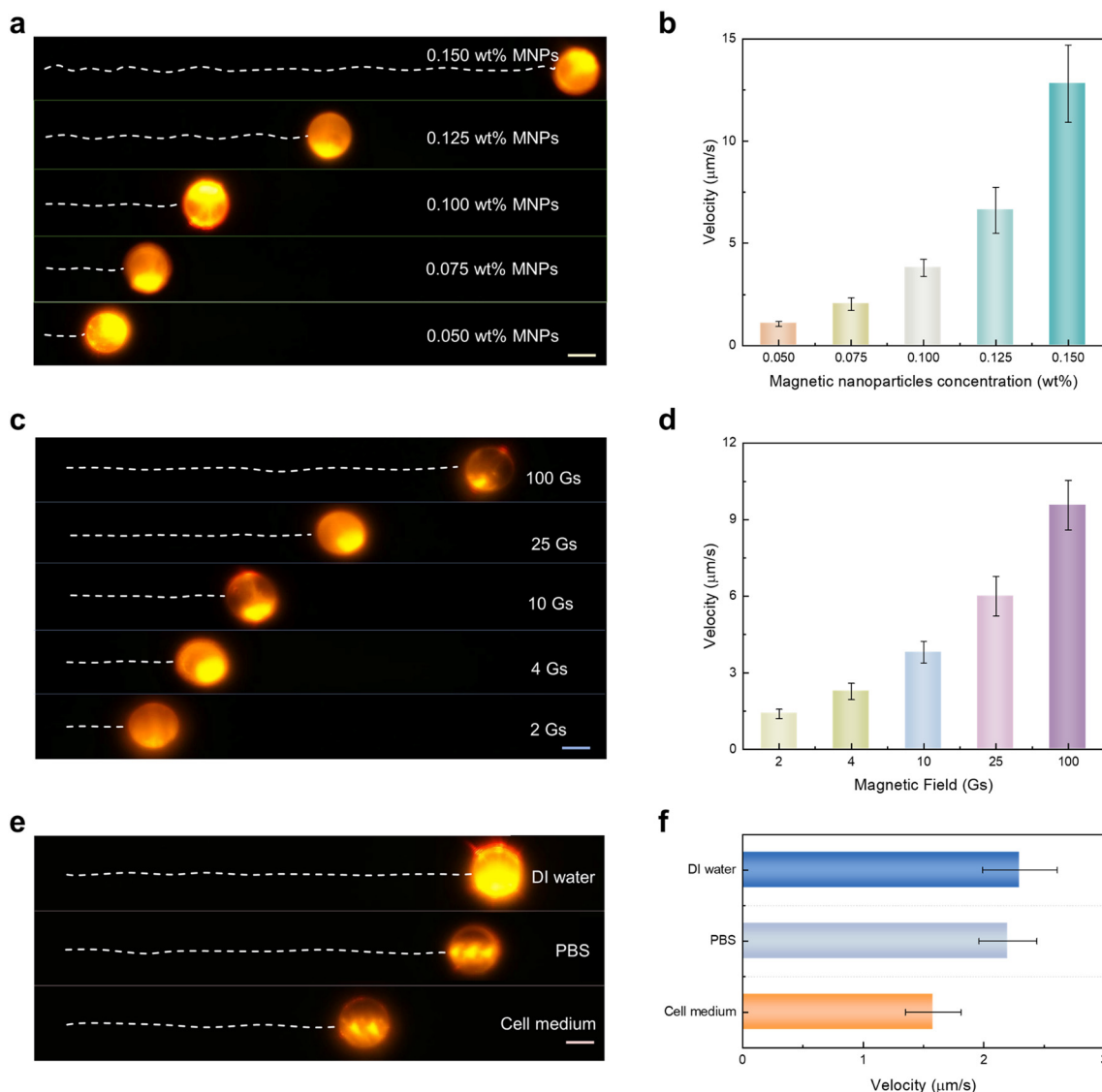
Fig. 2 (a and b) Motions and velocity of lasing micromotors under different magnetic nanoparticle concentrations. (a) Trajectories and (b) velocities recorded under a fixed time period (18 s) and magnetic field of 10 Gs. (c and d) Motions and velocity of lasing micromotors under different magnetic fields. (c) Trajectories and (d) velocities recorded under various external magnetic fields (with 0.1 wt% MNPs doped). (e and f) Motions and velocity of lasing micromotors propelling in different biological fluids (MNP concentration: 0.05 wt%, magnetic field: 10 Gs). (e) Image illustrating the propulsion (monitored 125 s) and (f) corresponding velocities in DI water, phosphate–buffered saline (PBS) solution, and cell culture medium. All scale bars: 20 μm.

and the lasing intensity remained stable. Besides linear motion, here, we demonstrate the ability of self-rotation in Fig. 1d and Video S2† by rotating the magnetic field. The position of the self-rotatory lasing micromotor as well as its lasing spectrum was recorded, as shown in Fig. 1d, respectively.

Next, we demonstrate the ability to manipulate the velocity of the lasing micromotor by changing its internal MNP concentration or altering external magnetic fields. As presented in Fig. 2a and corresponding Video S3,† the velocity of the lasing micromotor can be adjusted by loading different MNP concentrations inside the CLC droplet (note that the visualized colors of droplets appear different among Fig. 1 and 2. This is because they were measured under different microscopic camera systems due to the required field of view and imaging functions. A single point pump laser was used in Fig. 1, while a galvo-scanning laser pump was required to track the motors in a larger dimension in Fig. 2 and 3. However, the lasing spectra remained at the same wavelength band. More information on our optical setup can be found in "Materials and methods"). Under a fixed period of time and magnetic field of 10 Gs, lasing micromotors with higher MNP concentration presented a more significant propelled motion. Based on the trajectories shown in Fig. 2a, the average velocity increases accordingly as the concentration of MNPs increases (Fig. 2b). For each MNP concentration, three lasing micromotors were measured to obtain the average velocity. In addition, the lasing micromotor could be manipulated by external magnetic fields. Herein, different magnets were employed to investigate the dependence of applied magnetics strength. Under a fixed MNP concentration (0.1 wt%), Fig. 2c and Video S4† present the trajectories of lasing micromotors when applied under different magnetic fields. The average velocity increases accordingly as the magnetic field increases in Fig. 2d. Note that

the motion of lasing micromotors could be switched on and off by controlling the propulsion of external magnetic fields, as displayed in Fig. S4 and Video S5.† Through precise control of magnetic fields, the motions of the lasing micromotor can be fully controlled, including deceleration, acceleration, a complete stop, and subsequently reactivated.

We further investigated the propulsion performance in various types of biological fluids. Fig. 2e shows the trajectory of lasing micromotors moving forward in deionized (DI) water, phosphate-buffered saline (PBS), and cell medium (under fixed MNP concentration and magnetic field). The average velocity was measured to be 2.3 $\mu m\ s^{-1}$ in DI water, 2.2 $\mu m\ s^{-1}$ in PBS, and 1.58 $\mu m\ s^{-1}$ in cell medium, respectively. These differences can be attributed to increased environmental viscosity of biofluids, as presented in Fig. 2f.[8] Nevertheless, the intensity and structure of the lasing micromotor remain stable, indicating possible applications in biological and cellular environments.

By doping the corresponding luminescent dyes (Coumarin 6 (C6), 4-(dicyanomethylene)-2-methyl-6-(4-dimethylaminostyryl)-4H-pyran (DCM), and NR) into CLC lasing micromotors, laser emissions with green, yellow, and red wavelengths could be achieved. Fig. S5† presents the absorption and emission spectra of dyes used in this study. As exhibited in Fig. 3a, a 473 nm high-repetition-rate pulsed laser with a galvo-scanner was employed to track the quasi-real-time positions of multiple lasing micromotors in an aqueous solution. Multicolor letters "N" (red, NR), "T" (green, C6), and "U" (yellow, DCM) written by lasing micromotors were obtained through precise manipulation of magnet fields and directions. Individual frames recorded under each second are provided in ESI† Video S6. The images show the trajectory of lasing micromotors excited by the galvo-scanning mirror integrated with the high-repetition rate
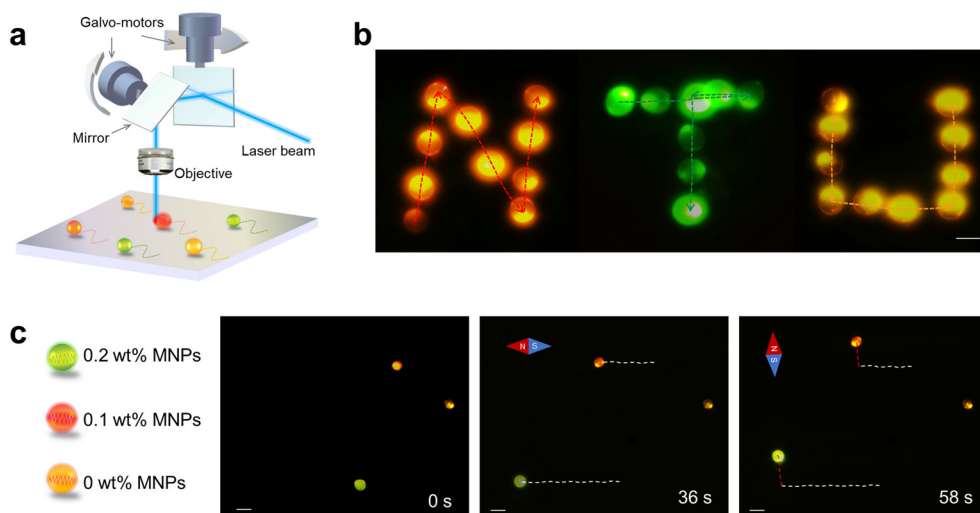
Fig. 3 (a) Illustration of the galvo-mirror laser scanning system for imaging the trajectories of multiple lasing micromotors. (b) Letters "N" (orange-red, NR), "T" (green, C6), and "U" (yellow, DCM) were written by the lasing micromotor. Dotted lines represented the trajectories of the corresponding lasing micromotor (Video S6†). Scale bar: 20 μm. (c) Multicolored micromotor exhibited different velocities. Lasing micromotors with 0.2 wt%, 0.1 wt%, and 0 wt% MNPs were doped with C6, NR, and DCM. Scale bar: 50 μm.

pulsed laser; the corresponding trajectories are marked in Fig. 3b. Note that the traces of lasing micromotors were formed by collecting in real-time under a high-speed camera and processed through image stacking algorithms. For each measurement, the pump laser was scanned in the *XY* plane, and the laser image was recorded by the CCD camera. A two-dimensional laser image was reconstructed by integrating all the time frames captured by the CCD camera (Fig. S6†).

To demonstrate the ability to selectively manipulate different lasing micromotors, here we prepared three CLC droplets encoded with different concentrations, each corresponding to a distinctive lasing wavelength. Fig. 3c shows different dyes that were used to encode lasing micromotors with different MNPs, including C6 (0.2 wt% MNPs), NR (0.1 wt%), and DCM (0 wt% MNPs), respectively. The trajectories were recorded and plotted in white-dashed lines when the magnetic field was applied toward the left during 1–36 s. Subsequently, the direction of the magnetic field was switched vertically from 37–58 s; the trajectories were then recorded in red dashed lines (37–58 s) (Video S7†). From Fig. 3c, we can observe that the yellow droplet (0% MNP) remained at its position, while the other two droplets presented different velocity behavior as a result of different MNP concentrations. Taking advantage of laser emission, lasing micromotors carrying different characteristics can be manipulated through encoded MNP concentrations and singled out by different lasing wavelengths.

Next, we investigated the potential applications of lasing micromotors by functioning as a localized stimulation emission light source in biological fluids. As shown in Fig. 4a, a green-laser emitting micromotor was exploited to excite red-emissive microdroplets. A Bodipy (2,8-diethyl-1,3,5,7-tetramethyl-9-phenylbipyrromethene difluoroborate)-doped lasing micromotor served as the donor, while an NR-doped droplet served as the acceptor. Under the guidance of a magnetic field, the distance between the green lasing micromotor and red-droplet can be precisely controlled. As a control group, the pump beam was fixed at a location as shown in Fig. 4b. One can see that no laser emission was detected from both droplets. When the green lasing micromotor was guided into the pump region, sharp lasing peaks from green emission bands were observed (Fig. 4c). As the green lasing approaches the red droplet with a distance of 1.4 μm apart, weak stimulated emissions were observed around 640–650 nm (Fig. 4d). The radiative WGM laser emission from the green droplet may excite the acceptor. When the green micromotor comes into contact with the red droplet, enhanced stimulated emission was observed in the bottom panel of Fig. 4d. This can be explained through cavity-mediated radiative energy transfer.[18,36,37] Owing to the close proximity and efficient energy transfer, the lasing intensity of the micromotor significantly decreased while the emission intensity of the red droplet increased simultaneously. On this basis, stimulated emission from red droplets could also be turned off by propelling away from the lasing micromotor. Fig. 4e demonstrates the ability to switch on and off the red stimulated emission over several cycles, indicating good reproducibility and stability of the lasing micromotor. Note that the intensity of the green lasing motor as well as red stimulated emission can be manipulated according to the distance between two objects. In addition, the laser modes can also be manipulated under precise control in the future. For instance, optical coupling between two lasing motors may result in single-mode lasing *via* the Vernier effect.[38–41]
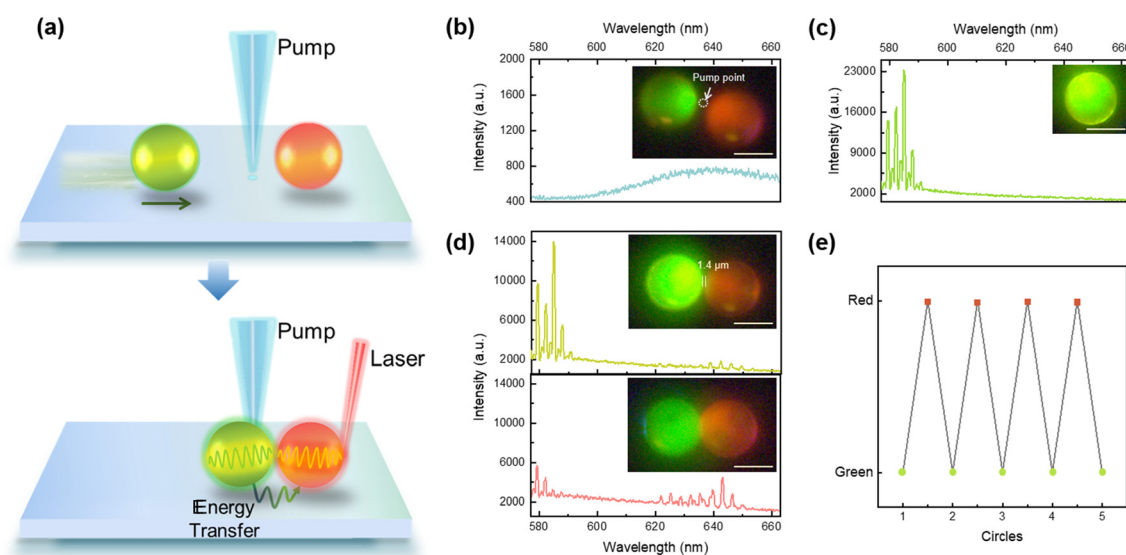
Fig. 4 (a) Illustration of the lasing micromotor used for switching on and off laser emissions. (b) Control group to evaluate the excitation effect on the NR-doped CLC microdroplet. (c) WGM lasing spectrum of the Bodipy-doped lasing micromotor alone. (d) Lasing spectra when the lasing micromotor (green) approaches the red CLC droplet. The inset shows the distance between two droplets: 1.4 μm (top), almost attached (bottom). Obvious WGM lasing emission from the acceptor (wavelength: 620–651 nm) can be found. (e) Laser switching (with green and red laser) emission by adjusting the motor. Scale bar: 20 μm.

Finally, we demonstrate the possibility of employing the lasing micromotor as a localized micro-laser source to stimulate or illuminate living cells in Fig. 5. Similar to the previous experiment in Fig. 4, a green laser-emitting lasing micromotor was exploited to excite fluorescently labeled live cells (red fluorescence from NR), as illustrated in Fig. 5a. Through the guidance of magnetic fields, the lasing micromotor could be guided to the membrane interface of the targeted cell (top panel). Excited fluorescence emission from the cell was obtained by cavity-enhanced radiative energy transfer from the lasing micromotor (bottom panel). Fig. 5b shows a brightfield image of a skeletal myoblast (C2C12 cell) with a C6-doped lasing micromotor adhered to its membrane surface. The corresponding fluorescence image captured under broadband green LED light is provided in Fig. 5c, demonstrating the successful labeling of the myoblast (red fluorescence emissions). Note that the LED-excited micromotor also appears red due to the broad fluorescence band of C6. In Fig. 5b and c, no pump laser was employed; hence no laser emission should be observed. Subsequently, in Fig. 5d and e, a pulsed laser with 470 nm was used for lasing micromotor excitation. As a control group in Fig. 5d, the position and intensity of the pump laser were fixed at a location to avoid direct excitation on the cell. When the lasing micromotor is propelled away from the cell, no signals from either the micromotor or the cell could be observed under 470 nm pump excitation (Fig. 5d). When the lasing micromotor adheres to the cell membrane, the fluorescently labeled cell could be excited by the green laser emitted from the micromotor, as presented in Fig. 5e. The inset images show some subcellular structures with a good signal-to-noise ratio, providing a side-illumination configuration that may exhibit additional stereoscopic and depth information. Note that here we demonstrate single cell stimulation (imaging); the same concept can be extended to multiple cell imaging by applying multiple lasing droplets and a galvo-scanner in Fig. 3.

Conclusions

Motor-like microlasers provide an alternative platform through the fusion of synthetic motors and optofluidic lasers. Tunability and reconfigurability are two major advantages that they can provide as compared to conventional solid approaches. One can change the optical properties of the motors by manipulating the materials of fluids and the structure of the optical resonator; for instance, the refractive index, emission wavelength, and optical gain can be adjusted by encapsulating arbitrary liquid gain materials. In addition to the fluorescent dyes used in this work, other liquid materials can also be applied to further extend the lasing wavelengths, *e.g.*, quantum dots and other organic materials or even biomaterials. Besides controlling the lasing micromotor with magnetic forces, other propelling forces such as enzymatic reactions, ultrasound, electrical forces, optical tweezers, and stimuli-responsive reactions could also be integrated with optofluidic lasing micromotors. In contrast to previous work published so far,[34] our work demonstrated stronger motion controllability in arbitrary dimensions and the ability to manipulate or monitor individual motors through lasing wavelength and thresholds. For the first time, we demonstrated the potential of using such motor-like lasers to function as an active probe in a biological environment.

To conclude, the concept of lasing micromotors was proposed, in which the motion and velocity could be fully modulated by adjusting either the internal MNP concentrations or external magnetic strengths. Precise control of lasing micromotors in X–Y directions, as well as rotatory motions, was achieved and evaluated in different biological solutions, including DI water, PBS solution, and cell medium. Although we understand that this concept is still very premature, here we introduced potential applications of lasing micromotors: (1) under the guidance of
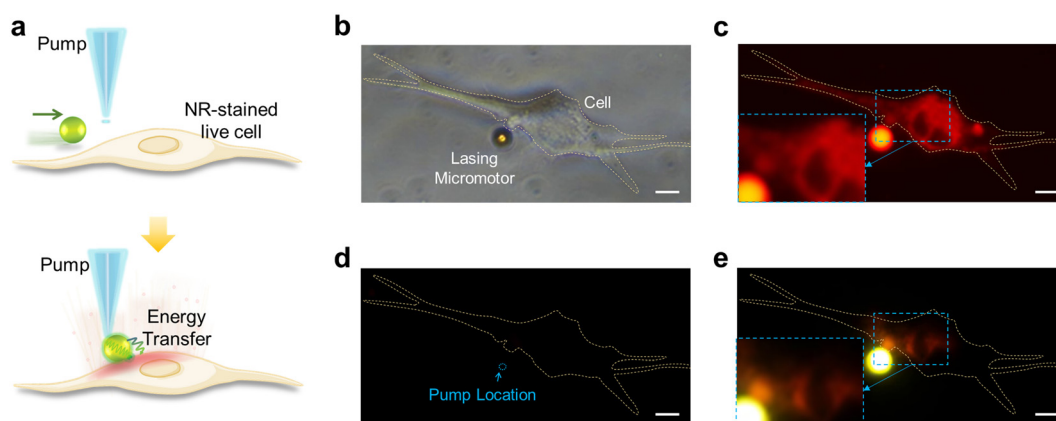
Fig. 5 (a) Schematic diagram of lasing micromotors used for live cell stimulation and imaging. (b) Brightfield and (c) corresponding fluorescence image (observed in 580–660 nm waveband). Illuminated by broadband green LED light, no laser emission involved in (c). Inset: Enlarged image at the cell-interface (diameter: 9 μm); (d) control group with no lasing motors existing. (e) Fluorescent emission from the live cell excited by the lasing micromotor. Inset: Enlarged image at the cell–droplet interface (the same position as in the inset of (c)). Yellow dashed lines: cell boundary. Scale bars: 10 μm.

a magnetic field, multicolored-encoded lasing micromotors could be employed for inkless laser writing and constructing microscale emitting patterns. Lasing micromotors encoded with different characteristics and functions were demonstrated. (2) Micromotors were utilized as laser switching probes by taking advantage of microcavity radiation, indicating that lasing micromotors may serve as versatile coherent light sources for micro-manipulation. (3) Micromotors were utilized as local laser sources to excite and illuminate subcellular features, providing a possible imaging modality in complex biological fluidics at single-cell resolution. (4) As an emerging platform, the possibility of moving these swimming micromotors in the air can be explored, at the same time, some difficulties need to be solved. For example, the formation of CLC sphere-shaped droplets is limited to the solution-based environment to maintain its spherical shape. Changing the shape of micromotors from droplets to hemisphere-shaped droplets on a superhydrophobic surface or other soft matter materials may be an efficient strategy.

Materials and methods

Chemical materials

4′-Pentyl-4-biphenylcarbonitrile was purchased from Sigma-Aldrich (#328510) as a nematic liquid crystal (5CB), and (S)-4-cyano-4′-(2-methylbutyl)biphenyl (CB15, Tokyo Chemical Industry) as a chiral dopant. MNPs (iron(II,III) oxide (Fe$_3$O$_4$)) with 50–100 nm particle size were purchased from Sigma-Aldrich (#637106). For the formation of CLC microdroplets with planar alignment, we used PVA (saponification 80 mol%) bought from Tokyo Chemical Industry (#P0804). The organic dyes used in this study were as follows: coumarin 6 (C6) (Sigma, #442631), Bodipy (Sigma, #795526), DCM (Tokyo Chemical Industry, #D2849), and NR (Sigma, #72485). Magnets were purchased from K&J Magnetics Inc. (#B222G-N52, #B333, #B444, #B666, and #B888).

Microfluidic device fabrication

Poly(dimethylsiloxane) (PDMS) prepared by mixing the pre-polymer and the curing agent at a ratio of 10 : 1 w/w was used for fabrication. After degassing in a vacuum desiccator for 1 h, the mixture was cured on the prepatterned silicon wafers. To form an irreversibly sealed microchannel, channels and glass slides were exposed to oxygen plasma under vacuum. Dimension information of microfluidic devices is provided in Fig. S7.†

Lasing micromotor preparation

The nematic liquid crystal and chiral dopant were mixed by a vortex mixer to form homogeneous CLC, and the chiral dopant concentration is 20 wt%. To represent lasing emission wavelengths, 1.4 mg C6, 1.22 mg Bodipy, 1.21 mg of DCM, and 1.27 mg of NR were added in 200 μL of CLC, respectively. MNPs with various concentrations were added

into dye-doped CLC subsequently. All the above mixtures were immersed in an ultrasonic bath for 25 min to gain homogeneous CLC samples. To prepare the uniform magnetic-actuated lasing micromotor, a home-built microfluidic chip was used. PVA solution, as the continuous water phase, from the two side channels surrounds the oil phase (MNPs-doped CLC). The oil phase periodically breaks in the orifice, and uniform CLC droplets are released into the outlet channel without any coalescence.

Acquisition of C2C12 cells

Mouse skeletal myoblast cell line C2C12 was cultured in DMEM supplemented with 10% FBS and 1% Pen/Strep. The cells were grown on a Petri dish in a humidified incubator at 37 °C and 5% CO$_2$. For NR-stained live C2C12 cells used in the experiments, the samples (cells) were firstly washed twice with PBS solution, then stained by NR solutions for 2 min, and finally washed with PBS solution for further laser experiments.

Optical system setup

An inverted microscopy system (Nikon Ti2) was employed for pumping the micromotor and collection of laser light. Optical laser pumping was achieved by a tunable pulsed laser (EKSPLA NT230) with 5 ns pulse duration (repetition rate: 50 Hz). For the C6-doped/Bodipy-doped micromotor, the pump wavelength was 470 nm; for the NR-doped micromotor, the pump wavelength was 530 nm. The pump energy density could be adjusted by a continuously variable neutral density filter (0.2–500 μJ mm^{-2}). The emission light was collected and sent into a charge-coupled device camera and imaging spectrometer (Andor Kymera 328i/Newton 970 EMCCD). For tracking the trajectories of lasing micromotors, the pump laser was replaced with a high repetition rate pulsed laser (RPMC 473 nm Microlaser SB1-473-3-5, 5 kHz, 2 ns pulse width). The laser passing through the 2D galvo scanner (Thorlabs, GVS102) scans in the x–y plane. Differences in the dynamic range and sensitivity of CCDs result in different colors in the figures, although all the micromotors were doped with the same concentration of NR. For clear illustration, we provided details of CCD used in our experiments.

Fig. 1(c and d) and 4(b–d): Basler aca1600-20uc (CCD); EKSPLA NT230 (pump laser).

Fig. 2(a, c, and e) and 3(b and c): Nikon, DS-Fi3 (CCD); RPMC 473 nm Microlaser SB1-473-3-5 (pump laser); Fig. 5(b–e): Nikon, DS-Fi3 (CCD); EKSPLA NT230 (pump laser).

Author contributions

Z. W., and Y.-C. C. conceived and designed the experiments; Z. W., L. S. and C. W. performed the optical experiments. K. K. C. and C. G. conducted the cellular preparation and experiments. S. F. and Z. G. designed and fabricated the microfluidic devices. Z. W., L. S., and Y.-C. C analyzed the

data. T. X. and T. L. provided useful advice. Z. W. and Y.-C. C. wrote the paper. Y.-C. C. supervised the whole research.

Conflicts of interest

The authors declare no conflicts of interest.

References

1 M. Safdar, S. U. Khan and J. Janis, *Adv. Mater.*, 2018, **30**, e1703660.
2 A. C. Hortelão, T. Patiño, A. Perez-Jiménez, À. Blanco and S. Sánchez, *Adv. Funct. Mater.*, 2018, **28**, 1705086.
3 Y. Zhang and T. H. Wang, *Adv. Mater.*, 2013, **25**, 2903–2908.
4 Z. Long, A. M. Shetty, M. J. Solomon and R. G. Larson, *Lab Chip*, 2009, **9**, 1567–1575.
5 J. Wang, B. J. Toebes, A. S. Plachokova, Q. Liu, D. Deng, J. A. Jansen, F. Yang and D. A. Wilson, *Adv. Healthcare Mater.*, 2020, **9**, e1901710.
6 X. Ma, A. C. Hortelao, A. Miguel-Lopez and S. Sanchez, *J. Am. Chem. Soc.*, 2016, **138**, 13782–13785.
7 S. Nocentini, C. Parmeggiani, D. Martella and D. S. Wiersma, *Adv. Opt. Mater.*, 2018, **6**, 1800207.
8 C. Gao, Z. Lin, D. Wang, Z. Wu, H. Xie and Q. He, *ACS Appl. Mater. Interfaces*, 2019, **11**, 23392–23400.
9 Z. Wu, T. Li, J. Li, W. Gao, T. Xu, C. Christianson, W. Gao, M. Galarnyk, Q. He, L. Zhang and J. Wang, *ACS Nano*, 2014, **8**, 12041–12048.
10 H. Xin, N. Zhao, Y. Wang, X. Zhao, T. Pan, Y. Shi and B. Li, *Nano Lett.*, 2020, **20**, 7177–7185.
11 Y. Li, X. Liu, X. Xu, H. Xin, Y. Zhang and B. Li, *Adv. Funct. Mater.*, 2019, **29**, 1905568.
12 X. Zhao, Y. Shi, T. Pan, D. Lu, J. Xiong, B. Li and H. Xin, *Nano Lett.*, 2022, **22**, 402–410.
13 R. María-Hormigos, A. Escarpa, B. Goudeau, V. Ravaine, A. Perro and A. Kuhn, *Adv. Mater. Interfaces*, 2020, **7**, 1902094.
14 D. Zhang, Y. Sun, M. Li, H. Zhang, B. Song and B. Dong, *J. Mater. Chem. C*, 2018, **6**, 12234–12239.
15 G. Salinas, I. A. Pavel, N. Sojic and A. Kuhn, *ChemElectroChem*, 2020, **7**, 4853–4862.
16 K. Hou, D. Guan, H. Li, Y. Sun, Y. Long and K. Song, *Sci. Adv.*, 2021, **7**, eabh3051.
17 Z. Wang, Y. Zhang, X. Gong, Z. Yuan, S. Feng, T. Xu, T. Liu and Y.-C. Chen, *Nanoscale Adv.*, 2020, **2**, 2713–2719.
18 Z. Yuan, Z. Wang, P. Guan, X. Wu and Y. C. Chen, *Adv. Opt. Mater.*, 2020, **8**, 1901596.
19 Y. C. Chen and X. Fan, *Adv. Opt. Mater.*, 2019, **7**, 1900377.

20 Y. Wang, S. Zeng, G. Humbert and H. P. Ho, *Laser Photonics Rev.*, 2020, **14**, 2000135.
21 Z. Wang, T. Xu, A. Noel, Y. C. Chen and T. Liu, *Soft Matter*, 2021, **17**, 4675–4702.
22 Y. Liu, A. Teitelboim, A. Fernandez-Bravo, K. Yao, M. V. P. Altoe, S. Aloni, C. Zhang, B. E. Cohen, P. J. Schuck and E. M. Chan, *ACS Nano*, 2020, **14**, 1508–1519.
23 A. Fernandez-Bravo, K. Yao, E. S. Barnard, N. J. Borys, E. S. Levy, B. Tian, C. A. Tajon, L. Moretti, M. V. Altoe, S. Aloni, K. Beketayev, F. Scotognella, B. E. Cohen, E. M. Chan and P. J. Schuck, *Nat. Nanotechnol.*, 2018, **13**, 572–577.
24 N. Martino, S. J. J. Kwok, A. C. Liapis, S. Forward, H. Jang, H.-M. Kim, S. J. Wu, J. Wu, P. H. Dannenberg, S.-J. Jang, Y.-H. Lee and S.-H. Yun, *Nat. Photonics*, 2019, **13**, 720–727.
25 M. Humar and S. Hyun Yun, *Nat. Photonics*, 2015, **9**, 572–576.
26 Z. Qiao, W. Sun, N. Zhang, R. Ang, W. Wang, S. Y. Chew and Y.-C. Chen, *Adv. Opt. Mater.*, 2021, **9**, 2101421.
27 Z. Qiao, H. Xu, N. Zhang, X. Gong, C. Gong, G. Yang, S. Y. Chew, C. Huang and Y.-C. Chen, *Adv. Sci.*, 2022, **9**, 2103550.
28 M. Schubert, L. Woolfson, I. R. M. Barnard, A. M. Dorward, B. Casement, A. Morton, G. B. Robertson, P. L. Appleton, G. B. Miles, C. S. Tucker, S. J. Pitt and M. C. Gather, *Nat. Photonics*, 2020, **14**, 452–458.
29 T. Pan, D. Lu, H. Xin and B. Li, *Light: Sci. Appl.*, 2021, **10**, 124.
30 D. Septiadi, V. Barna, D. Saxena, R. Sapienza, D. Genovese and L. De Cola, *Adv. Opt. Mater.*, 2020, **8**, 1901573.
31 K. Sasaki, *Mater. Sci. Eng., B*, 1997, **48**, 147–152.
32 K. Sasaki, H. Fujiwara and H. Masuhara, *J. Vac. Sci. Technol., B: Microelectron. Nanometer Struct.–Process., Meas., Phenom.*, 1997, **15**, 2786–2790.
33 A. Jonáš, Z. Pilát, J. Ježek, S. Bernatová, P. Jedlička, M. Aas, A. Kiraz and P. Zemánek, *ACS Appl. Mater. Interfaces*, 2021, **13**, 50657–50667.
34 L.-J. Chen, L.-L. Gong, Y.-L. Lin, X.-Y. Jin, H.-Y. Li, S.-S. Li, K.-J. Che, Z.-P. Cai and C. J. Yang, *Lab Chip*, 2016, **16**, 1206–1213.
35 C. Wang, C. Gong, Y. Zhang, Z. Qiao, Z. Yuan, Y. Gong, G.-E. Chang, W.-C. Tu and Y.-C. Chen, *ACS Nano*, 2021, **15**, 11126–11136.
36 D. Okada, T. Nakamura, D. Braam, T. D. Dao, S. Ishii, T. Nagao, A. Lorke, T. Nabeshima and Y. Yamamoto, *ACS Nano*, 2016, **10**, 7058–7063.
37 A. Hendra, H. Takeuchi, O. Yamagishi, M. Oki, M. I. Morimoto and Y. Yamamoto, *Adv. Funct. Mater.*, 2021, **31**, 2103685.
38 C. Zhang, C.-L. Zou, H. Dong, Y. Yan, J. Yao and Y. S. Zhao, *Sci. Adv.*, 2017, **3**, e1700225.
39 Y. Du, C.-L. Zou, C. Zhang, K. Wang, C. Qiao, J. Yao and Y. S. Zhao, *Light: Sci. Appl.*, 2020, **9**, 1–9.
40 R. Duan, Z. Zhang, L. Xiao, X. Zhao, Y. T. Thung, L. Ding, Z. Liu, J. Yang, V. D. Ta and H. Sun, *Adv. Mater.*, 2022, **34**, 2108884.
41 V. D. Ta, R. Chen and H. Sun, *Adv. Opt. Mater.*, 2014, **2**, 220–225.